JGR Planets

RESEARCH ARTICLE
10.1029/2020JE006609

Key points:

- Experiments constrain the temperature of fumarolic Apollo 16 "Rusty Rock" alteration to 580 ± 50°C
- The phase assemblage of $FeCl_2$ and (Zn,Fe)S constrains the composition of the fumarolic gas at 600°C
- Gas deposition and gas-solid metal reaction experiments reproduce the "Rusty Rock" alteration phases $FeCl_2$ and (Zn, Fe)S

Supporting Information:

- Supporting Information S1

Correspondence to:
C. Renggli,
renggli@uni-muenster.de

Citation:
Renggli, C. J., & Klemme, S. (2021). Experimental investigation of Apollo 16 "Rusty Rock" alteration by a lunar fumarolic gas. *Journal of Geophysical Research: Planets*, *126*, e2020JE006609. https://doi.org/10.1029/2020JE006609

Received 3 JUL 2020
Accepted 5 DEC 2020

Author Contributions:

Conceptualization: C. J. Renggli
Data curation: C. J. Renggli
Formal analysis: C. J. Renggli
Funding acquisition: S. Klemme
Investigation: C. J. Renggli
Methodology: C. J. Renggli
Project Administration: C. J. Renggli, S. Klemme
Resources: S. Klemme
Software: C. J. Renggli
Supervision: S. Klemme
Validation: C. J. Renggli
Writing – original draft: C. J. Renggli
Writing – review & editing: C. J. Renggli, S. Klemme

Experimental Investigation of Apollo 16 "Rusty Rock" Alteration by a Lunar Fumarolic Gas

C. J. Renggli[1] and S. Klemme[1]

[1]Institut für Mineralogie, Universität Münster, Münster, Deutschland

Abstract The Apollo 16 sample 66095, named "Rusty Rock", is enriched in volatile and moderately volatile elements. The impact melt breccia is characterized by abundant Fe-rich sulfide and chloride alteration phases, including FeS, ZnS, and $FeCl_2$. These phases have previously been interpreted to be the result of fumarolic alteration of the breccia. Here we present the results of two different experimental approaches, which aim to constrain the temperature conditions and the process under which the "Rusty Rock" alteration formed. The first experimental set-up assumes that the metals Zn, Cu, and Fe were introduced into the rock by a C-O-S-Cl gas phase, and that the Fe-rich sulfides and chlorides were deposited from this gas phase. This "gas deposition" experiment suggests that the alteration assemblage formed over the temperature range of 538–638 ± 5°C. The second experimental set-up simulates a scenario, where Fe metal particles in the lunar rock react with a Zn-C-O-S-Cl gas phase at six different temperatures between 396 ± 5°C and 1,005 ± 5°C. This latter "metal reaction" experiment resulted in the formation of sulfide and chloride coatings on the Fe metal chips. The "Rusty Rock" alteration phases $FeCl_2$ and (Zn,Fe)S were abundantly present in the coating of the Fe metal chip reacted at 580 ± 10°C. Both experiments lead to results which are in agreement, providing a temperature of 580 ± 50°C for the fumarolic alteration on the Moon, as observed in the Apollo 16 "Rusty Rock".

Plain Language Summary The Apollo 16 sample 66095, colloquially named "Rusty Rock", is an unusual lunar rock which is enriched in volatile elements such as sulfur and chlorine. We investigate two processes by which sulfides and chlorides may form in a lunar fumarolic system, by conducting experiments in evacuated silica glass tubes at reducing conditions. First, we assume that metals and volatiles (Zn, Cu, Fe, S, and Cl) are all deposited from a gas phase (gas deposition experiments), and second, we assume that Fe metal is already present in the rock and that the Fe altered by the introduction of a Zn-S-Cl-bearing gas phase (metal reaction experiment). In both experimental setups we observe the formation of "Rusty Rock" alteration phases $FeCl_2$ and (Zn, Fe)S at 580 ± 50°C, constraining the temperature of fumarolic alteration recorded in the Apollo 16 sample 66095. Hence, our experiments confirm that the characteristic S- and Cl-rich minerals found in the lunar "Rusty Rock" were formed by a lunar fumarole. More broadly, lunar metal deposits may be associated with ancient fumarolic processes.

1. Introduction

The Apollo 16 "Rusty Rock" 66095 is a unique lunar sample which is highly enriched in the volatile elements S and Cl and in moderately volatile trace metals such as Tl, Br, Cd, Sn, Zn, Pb, Rb, Cs, Ga, B, and Li (Day et al., 2017, 2019; Krähenbühl et al., 1973; Shearer et al., 2014; Taylor et al., 1973). This volatile element enrichment of the "Rusty Rock" is in contrast to the vast majority of lunar samples which are generally very volatile depleted relative to terrestrial magmatic rocks (e.g., McCubbin et al., 2015).

Sample 66095 is a fine-grained impact melt breccia with lithic clasts, including anorthosite, troctolite, basalt and a minor KREEP-like component. The lithic clasts further contain metallic iron-nickel grains. These grains are commonly altered on the rims to (Fe, Ni)Cl_2, FeO (OH, Cl), FeS, and occasional ZnS (El Goresy et al., 1973; Hunter and Taylor, 1981a, 1981b; Shearer et al., 2014; Taylor et al., 1973, 1974). The alteration occurs on the surface of the rocks as well as the interior, suggesting that it was not a secondary process that occurred after sampling, in the spacecraft or on Earth (Meyer, 2009). Similar alteration features were observed in more than 20 different Apollo 16 samples (Jean et al., 2016; Taylor et al., 1973). This suggests that the alteration is a regional lunar process, rather than limited to sample 66095. Sulfidation (sulfide formation

via gas-solid reactions) is not only associated with FeNi grains, but it also occurs disseminated in veins and replacement textures of olivine and pyroxene in Apollo 16 rocks (Colson, 1992; Norman, 1981; Norman et al., 1995; Shearer et al., 2012). This underlines the broader importance of the "Rusty Rock", which provides a unique insight into the transport of volatile elements in the lunar crust.

Recent work has highlighted unique isotopic signatures of the Apollo 16 "Rusty Rock" 66095, providing insights into the origin of enriched volatile elements (Day et al., 2017, 2019; Shearer et al., 2014). The "Rusty Rock" is one of the most S-rich Apollo 16 samples, and with $\delta^{34}S = +1.9\%$ one of the most isotopically light lunar samples (Kerridge et al., 1975). Other lunar samples with light $\delta^{34}S$ compositions include volatile coatings on Apollo 17 pyroclastic glass beads and troilite replacement veins in Apollo 16 breccias (Shearer et al., 2012). Because the light S isotopes preferentially partition into a gas phase, isotopically light $\delta^{34}S$ in 66095 sulfides indicate that they deposited from a volcanic or fumarolic gas (Shearer et al., 2012, 2014). The Cl isotopic composition of 66095, on the other hand, is heavy with respect to lunar igneous rocks, with $\delta^{37}Cl$ ranging from +14.0% to +15.6% (Gargano et al., 2020; Sharp et al., 2010; Shearer et al., 2014). Apart from lunar apatites (Ustunisik et al., 2015; Wang et al., 2012), these are the heaviest Cl isotopic compositions measured in lunar samples (Shearer et al., 2014). As the overall Cl isotopic composition of the Moon was inferred to be similar to that of the Earth, the occurrence of much heavier isotopic compositions was attributed to the volatilization of metal halides (Gargano et al., 2020; Sharp et al., 2010; Shearer et al., 2014). These metal halides were deposited from the gas phase on pyroclastic glass beads, and in altered regolith and breccia such as 66095 (Shearer et al., 2014). The isotopic composition of Zn supports the interpretation of S and Cl isotopic compositions and the $\delta^{66}Zn$ composition of the "Rusty Rock" reveals the lightest isotopic signature of Zn recorded in any sample analyzed, with $\delta^{66}Zn = -13.7\%$ (Day et al., 2017). This light isotopic signature was interpreted to be caused by degassing from a volatile-depleted Moon and condensation in the lunar regolith and on the Moon's surface (Day et al., 2017, 2019). Note that Cu and Fe isotopic compositions of 66095 are not fractionated and are within the range of normal lunar mare basalts ($\delta^{65}Cu = 0.9\%$, $\delta^{56}Fe = 0.1\%$; Day et al., 2019). Iron is considered a non-volatile element but Cu is moderately volatile (Lodders, 2003; Norris & Wood, 2017; Sossi & Fegley, 2018; Sossi et al., 2019) so that stable Cu isotopes should have been fractionated if Cu had been deposited from a gas phase in the "Rusty Rock". In a lunar volcanic gas at 1 bar and 1200°C, Zn is two orders of magnitude more volatile than Cu, and four orders of magnitude more volatile than Fe (C. J. Renggli et al., 2017).

Two different mechanisms are conceivable for the formation of the observed sulfide and chloride alteration in the "Rusty Rock" samples. In the first scenario, all metals (i.e., Zn, Cu, and Fe), together with S and Cl, were introduced into the rock by a fumarolic gas phase, and this caused deposition of metal sulfides and chlorides (gas deposition process). For example, in such a process lawrencite could be introduced into the "Rusty Rock" as a gas according to the reaction $FeCl_{2(g)} = FeCl_{2(s)}$ (Colson, 1992). Similarly, Zn and Cu could be introduced as chloride, sulfide or elemental gas species and deposited under the same conditions as $FeCl_2$. This process would be recorded in the "Rusty Rock" by light isotopic signatures of the metals and the isotopically light Zn isotopes support this process (Day et al., 2017). However, the Cu and Fe isotopes are not isotopically light (Day et al., 2019) and hence this process does not account for the Cu and Fe isotopic signatures of 66095. In a second scenario, the metals Fe and Cu were not introduced by the gas phase, but instead, they were present in the rock prior to gas metasomatism, and hence the metals Cu and Fe reacted with a gas phase to form sulfides and chlorides (metal reaction process). Based on the isotopic composition, the latter mechanism was proposed to explain the alteration of Cu and Fe in the "Rusty Rock" (Day et al., 2019).

In both mechanisms, a S- and Cl-bearing gas phase causes the alteration, either by introducing the metals, or by reacting with the metals in the rock to cause the sulfidation and chlorination. The gas-solid reactions may have occurred in ejecta blankets (Haskin & Warren, 1991) with volatiles sourced from comets or meteorites, or mobilized from the crust (El Goresy et al., 1973; Papike et al., 1991). Norman et al. (1995) first proposed that the source of sulfidation in Apollo 16 ferroan noritic anorthosites was driven by anhydrous C-O-S-Cl vapors, derived from shallow magmatic sources in the lunar crust. The role of a S-rich and H-poor gas phase was supported by Shearer et al. (2012). Similarly, Shearer et al. (2014) suggested that $FeCl_2$, FeS, and ZnS in the "Rusty Rock" formed by a H-poor C-O-S-Cl gas, without a major extra-lunar contribution. Consequently, we conduct our experiments in a H-free system.

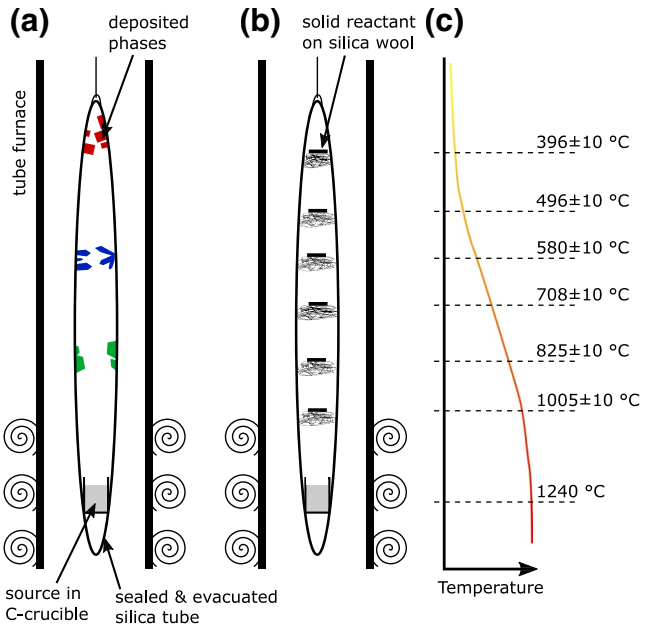

Figure 1. Illustration of the experimental setup in a vertical tube furnace. (a) Gas deposition experiment. The source in the hot zone of the furnace volatilizes and different phases (shown in green, blue and red) are deposited along the temperature gradient within the silica glass tube. (b) Metal reaction experiment. The Fe metal chips were placed on SiO_2 glass wool spacers at 396 ± 10, 496 ± 10, 580 ± 10, 708 ± 10, 825 ± 10, and 1,005 ± 10 °C; (c) schematic of the furnace temperature gradient with temperatures at which the Fe metal chips were placed within the tube.

Our aim is to investigate these gas deposition and metal reaction processes proposed for the "Rusty Rock" alteration experimentally, and constrain the temperature conditions under which the "Rusty Rock" alteration ($FeCl_2$, FeS, and ZnS) formed. Furthermore, we aim to put constraints on the fumarolic gas composition and test if the two mechanisms discussed above (deposition of Fe from the gas phase vs. in situ reaction with a C-O-S-Cl gas) are viable. For this purpose we used two different experimental approaches, simulating the different proposed alteration mechanisms, where the first approach assumes that all major elements of the alteration assemblage (i.e., Zn, Fe, Cu, Cl, and S) were transported by a gas phase to form deposits along a temperature gradient (gas deposition experiment), essentially identical to the formation of mineral deposits from fumarolic gases (Renggli & Klemme, 2020). The second approach assumes that the Fe metal was already present in the rock and reacted with a C-O-S-Cl gas phase (metal reaction experiment). In this experiment we also include Zn in the gas phase due to the evidence from light δ^{66}Zn in the "Rusty Rock", suggesting deposition from a gas phase (Day et al., 2017).

2. Methods

2.1. Experimental Rationale

We conducted two different gas-solid reaction experiments in evacuated silica glass tubes (Figure 1). We adopted the experimental setup from Renggli & Klemme (2020), where we showed that these types of experiments can reproduce sulfide and chloride deposits in observed in terrestrial fumaroles. The experimental set-up follows, in principle, Nekvasil et al. (2019), where a volatile element-rich source material is placed in an evacuated silica glass tube in the hot zone of a furnace. The volatile and moderately volatile elements are mobilized and transported in the gas phase, and minerals are deposited in colder parts along the furnace temperature gradient. The ~30 cm long silica glass tube (Figure 1) is placed in a vertical furnace so that the starting material is in the hot zone of the furnace. The furnace has a strong temperature gradient from the hot zone to the top of the furnace (Figure 1) and, hence, temperatures within the long glass tubes range from 1240°C, to 316°C at the top of the glass tube (Supporting Information S1; Renggli and Klemme, 2020). Overall, the experimental set-up, which is used to simulate the transport of metals in fumarolic gases on the Moon, is similar to natural fumaroles, characterized by large gradients in temperature and variations in redox conditions, and gas composition with time.

Our set-up does not allow precise control of the redox conditions in our experiments, as in conventional gas-mixing furnaces. However, our experimental results allow us to constrain the dynamic evolution of the gas phase and the redox conditions during the runs. As our starting material is placed in a graphite cup, the system in the hot zone (at 1240°C) is graphite saturated so that fO_2 cannot exceed the C-CO buffer (log-$fO_2 = -16.9$ at 1240°C and 1 bar). This buffer assemblage is only operational if oxygen is present. In colder parts of the experimental glass tubes the system remains reducing. Our results below show that metallic phases (e.g., Cu-whisker or Fe-metal chips) and no metal oxides are present, which constrains the redox conditions at lower temperatures to below the iron-wüstite (IW) buffer (see Section 4.1).

All experiments were conducted using evacuated and sealed silica glass tubes at an initial internal pressure of 10^{-5} bar. The silica glass tubes were suspended in a vertical tube furnace (Gero GmbH), so that the starting material was placed in the hot zone of the furnace, that is, 1240°C. The furnace had a temperature gradient of 900°C from the hot zone to the top of the silica glass tube (Figure 1, SupportingInformation S1), measured at 1 cm steps with a type B thermocouple. The temperature gradient is not linear along the tube, such that the 1 cm tube segments cover temperature ranges from 15°C at the high and low temperature ends, to 65°C where the gradient is steep around 700°C (see Renggli and Klemme 2020). We estimate a

Table 1
Composition of the Experimental Charges of the Gas Deposition and Metal Reaction Experiments

	Gas deposition experiment		Metal reaction experiment	
	Molar abundances	Weight g	Molar abundances	Weight g
ZnO	1	0.0068 (1)		1
FeS	1	0.0073 (1)	–	–
CuS	1	0.0080 (1)	–	–
$MgCl_2$	3	0.0239 (1)	1	0.0185 (1)
S	–	–	1	0.0062 (1)
C	4	0.0040 (1)	4	0.0094 (1)
Total	–	0.05	–	0.05

Note. The table shows nominal molar concentrations of the reagent mixtures and weighed-in values.

temperature error associated with the preparation of the gas deposition experiments of ±5. This uncertainty results from the placement of the silica tube in the furnace and the cutting of the tube into segments after the experiments. All experiments were run for 24 h. The starting material mixtures reacted at high temperature (1240°C) to form a gas phase that subsequently moved upwards along the temperature gradient over the duration of the run (Nekvasil et al., 2019). The amount of starting materials in the pellets was limited to 0.05 g. This quantity was chosen to avoid an over pressurization of the ampules ($P < 3$ bar), assuming that the entire pellet material was in the gas phase at 1250°C and give the inner volume of the sealed ampules (4 mm inner diameter, ~3,770 mm^3, see Renggli and Klemme 2020). The pressure in the experiments is not constant and evolves with time. Initially, as the volatile elements form a gas phase the pressure increases and rapidly equilibrates throughout the ampule, and gas species move along the temperature gradient by Soret diffusion (Nekvasil et al., 2019). As the solid phases begin to deposit from the gas phase on the silica glass tube wall, the pressure decreases again (Renggli and Klemme, 2020).

2.2. Experiments

Our starting material mixtures consisted of reagent grade oxides, sulfides, and chlorides as the volatile sources for the experiments, instead of synthetic silicate melts (Nekvasil et al., 2019; Ustunisik et al., 2019), to produce larger amounts of transported metals (Renggli and Klemme, 2020). The reagents were pressed into pellets (2 mm diameter) in a pellet press and at room temperature. The pellets were subsequently dried at 50°C over night and placed in graphite crucibles at the bottom of the silica glass tubes.

The first type of experiments, which we call "gas deposition experiments", simulates the transport of Zn, Cu, and Fe in a C-O-S-Cl gas and the resulting deposition of sulfide and chloride phases (Renggli and Klemme, 2020). The starting material was a mixture of ZnO, FeS, CuS, $MgCl_2$, and C in the relative molar abundances of 1-1-1-3-4 (Table 1), pressed into a 50 mg pellet and placed in an open graphite crucible, which was then placed at the bottom of a 30 cm long evacuated silica glass tube. Upon heating, the volatile reagents in the pellet form a gas (at 1240°C) with equal molar concentrations of Zn, Fe, and Cu, and equal molar concentrations of S and Cl. MgO was the only solid that remained in the graphite crucible after the experiment (Supporting Information S2).

In the second type of experiments, which we call "metal reaction experiments," we investigated the reaction of Fe metal with a Zn-C-O-S-Cl gas phase at 396 ± 10, 496 ± 10, 580 ± 10, 708 ± 10, 825 ± 10, and 1005 ± 10°C. These temperatures reflect the positions of the metal chips relative to the temperature gradient in the tube furnace at 7, 11, 13, 15, and 21 cm from the top of the furnace respectively (Table 2, Supporting Information S1), with a ±10°C temperature uncertainty resulting from the positioning of the tube in the furnace. As the source of volatiles, a pellet containing a mixture of ZnO, $MgCl_2$, S, and C in the relative molar abundances of 1-1-1-4 (Table 1) was pressed and placed in an open graphite crucible in the evacuated silica glass tube. In this experiment, volatilization of the starting material pellet forms a gas with relative abundances of Zn:S:Cl = 1:1:2. After the experiment the remaining pellet only consisted of MgO (Supporting Information S2), which is evidence for complete volatilization of Zn, S, and Cl. Iron metal chips with diameters of ~1 mm were placed on silica glass wool spacers along the tube prior to the evacuation of the tube. The contact of the Fe metal chips with the silica glass wool resulted in the formation of minor amounts of Fe_2SiO_4.

The silica glass tubes were lifted out of the furnace and quenched in cold water. The quenched tubes were cold within less than 10 s, minimizing secondary alteration within the tubes. The tubes were then cut in 1 cm long segments, corresponding to the position of the tubes relative to the temperature gradient in the furnace (Supporting Information S1). The tubes were cut to a precision of ±1 mm. The samples were immediately placed in an evacuated desiccator in order to avoid alteration by exposure to the humidity in the air

Table 2
Experimental Conditions and Positions of Fe Metal Chips Along the Silica Tube in the Metal Reaction Experiment

	Distance from top of tube (cm)	Temperature (°C)
a	7	396 ± 10
b	11	496 ± 10
c	13	580 ± 10
d	15	708 ± 10
e	17	825 ± 10
f	21	1005 ± 10
Volatile source	31	1240 ± 10
Tube length	–	28 cm
Duration	–	24 h

Note. Temperatures were measured with a type B thermocouple in the vertical tube furnace in 1 cm steps prior to the experiments.

(Dalby et al., 2018). Aliquots of the reacted Fe metal chips were embedded in epoxy resin and prepared as polished cross-sections. The mounts were polished dry without water to avoid hydration of the samples; however, the chlorides partially hydrated during sample preparation.

All samples were characterized with a JSM-6610 Series Scanning Electron Microscope (SEM). The silica tube segments with the sulfide and chloride deposits on the inner silica glass tube wall were analyzed without carbon coating using the low-vacuum capability of the SEM at 50 Pa. This allowed a minimization of sample exposure to ambient air and modification during sample preparation. The cross-sectioned samples were carbon coated and analyzed and imaged at high-vacuum using the Back-Scattered Electron (BSE) detector. All Energy-Dispersive X-Ray spectroscopy (EDS) analysis (both of the reacted surfaces and the cross-sectioned samples) were done at an acceleration voltage of 20 kV and a working distance of 10 mm, using the JEOL EDS analysis station with a dry silicon drift detector. The JEOL software performs and automated EDS peak identification and integrates the spectra to provide semi-quantitative atomic abundances. Due to the chemical simplicity of our experimental system, no significant peak overlap is observed in the EDS spectra, allowing the integration of the spectra and the extraction of the compositions of the experimental phases. We analyzed each observed phase 5–10 times on different grains with varying orientations (e.g., Zelenski et al. 2020), and provide standard deviations. We report the results of the EDS analysis as atomic% (Table 3 and Table 4).

3. Results

3.1. Gas Deposition Experiments

We observe eight different phases deposited on the inner wall of the silica glass tube, over the entire temperature range from 330 to 1240°C (Figure 2, Table 3). With the exception of forsterite (Mg_2SiO_4), which forms as the product of a reaction of the starting material with the silica glass tube, the phases were deposited from the Zn-Fe-Cu-C-O-S-Cl gas. We observe forsterite only at high temperatures ($T > 698 \pm 5$°C) with grain sizes of up to 20 μm. This suggests that minor amounts of the $MgCl_2$ in the starting material were transported in the gas phase and reacted with the hot silica glass tube wall. The only chemical compound remaining in the graphite crucible after the experiment is MgO, suggesting that gas phase transport of Mg was a minor process. The MgO forms a dense pellet with grain sizes of up to 20 μm (Supporting Information S1). Phases deposited from the gas phase are spread over almost the entire silica tube from 330 to 1140 ± 5°C, with little overlap of different phases (Figure 3).

Chalcocite (Cu_2S) occurs between 878 ± 5 and 1140 ± 5°C and forms tabular grains often deposited in patches or groups of multiple single crystals (Figures 2a and 2b). Below 1000 °C the crystals form increasingly well-developed crystal faces, whereas the typical habit of chalcocite crystals is more rounded at higher temperatures, especially in the case of crystals deposited near the melting point of Cu_2S at 1130°C. The crystals have diameters of up to 60 μm and are commonly associated with higher abundances of forsterite on the tube wall. All chalcocite crystals show the growth of Cu-metal whiskers extruding from their surface (Figure 2b). The whiskers have lengths of up to 10 μm and are composites of copper fibers with sub-micron diameters. At 698 ± 5–830 ± 5°C (Figure 3), we observe an unidentified Fe-Cu-S-Cl phase. These rare crystals have diameters of ∼40 μm and well-developed triangular crystal faces.

The largest quantities of metal sulfide and chloride deposits occur over the relatively narrow temperature range of 540 ± 5–700 ± 5°C (Figure 3). In this narrow temperature range, we observe the phases described in the Apollo "Rusty Rock", including FeS, lawrencite ($FeCl_2$), and wurtzite (ZnS). FeS (presumed troilite; 638 ± 5–698 ± 5°C) forms platy crystals and occurs together with lawrencite (Figure 2d). The FeS plates have diameters of up to 200 μm. Lawrencite occurs over a wider temperature range of 538 ± 5–698 ± 5°C

Table 3
Semi-quantitative EDS Analysis of the Observed Phases in the "Gas Deposition Experiment" Given in Atomic %

		S	Cl	Fe	Cu	Zn
Temperature (°C)	Phase	Atomic %	Atomic %	Atomic %	Atomic %	Atomic %
300–538	$ZnCl_2$	n.d.	59.0 (1.7)	0.9 (0.7)	n.d.	39.9 (1.9)
498–538	Zn-Cl-S	22.8 (1.3)	30.8 (6.3)	0.5 (0.2)	n.d.	45.9 (7.3)
538–587	ZnS	43.0 (2.1)	6.5 (0.7)	3.7 (0.4)	0.8 (0.1)	46.0 (2.1)
538–698	$FeCl_2$	1.9 (2.2)	61.1 (3.5)	36.6 (1.3)	n.d.	0.3 (0.1)
638–698	FeS	44.4 (1.9)	4.5 (2.2)	50.0 (2.7)	0.9 (0.3)	n.d.
698–830	Cu-Fe-Cl-S	31.5 (3.0)	20.5 (3.2)	16.2 (3.9)	31.6 (3.5)	n.d.
878–1140	Cu_2S	35.0 (2.5)	2.8 (1.0)	6.4 (0.8)	55.7 (2.0)	n.d.
878–1140	Cu (whiskers)	5.1 (2.7)	2.0 (1.3)	2.4 (1.4)	90.5 (3.7)	n.d.

Note. Standard deviations of the analyses are given in brackets. Backscattered electron images of the analyzed phases are shown in Figure 2; n.d., not detected, that is, below the detection limit.

(Figure 3). Where lawrencite coexists with FeS (Figure 2d) the crystals are small, with prismatic grains up to 10 μm in length. At slightly lower temperature (>638 ± 5°C) the lawrencite forms large platy grains (Figure 2e). Between 538 ± 5 and 587 ± 5°C, we observe a sharp boundary between a lawrencite and wurtzite dominated section (Figure 2f). In the wurtzite dominated section, we observe occasional triangular, platy $FeCl_2$ grains (Figure 2g). The occurrence of wurtzite is limited to a narrow temperature range of 538 ± 5–587 ± 5°C (Figure 3). The typical hexagonal shape of wurtzite is only occasionally observed, but here we find that it forms dense aggregations of intergrown ZnS crystals (Figure 2g). Below 538 ± 5°C, we only observe Zn-phases and no Cu- or Fe-bearing minerals. Below 498 ± 5°C, the only phase observed is $ZnCl_2$ (Figure 3). $ZnCl_2$ is highly deliquescent and rapidly absorbs enough water from the atmosphere to form an aqueous solution, once exposed to air. This process occurs within less than 5 min in the relatively humid air of Münster in the summer, apparent in all samples where $ZnCl_2$ is present (Figure 2i). Finally, in the transitional temperature range between 498 ± 5 and 538 ± 5°C (Figure 3), we observe an unidentified Zn-phase containing both S and Cl (Figure 2h).

Table 4
Semi-quantitative EDS Analysis of the Observed Mineral Phases in the "Metal Reaction Experiment" Given in Atomic %

		S	Cl	Fe	Zn
Temperature (°C)	Phase	Atomic %	Atomic %	Atomic %	Atomic %
396	$FeCl_2$	n.d.	65.3 (2.2)	34.1 (2.1)	n.d.
496	$FeCl_2$	3.4 (2.2)	59.9 (6.4)	19.8 (3.9)	16.9 (1.6)
580	$FeCl_2$	0.9 (0.6)	61.1 (3.8)	28.4 (5.2)	9.6 (1.9)
580	(Zn, Fe)S	49.5 (0.3)	4.4 (1.1)	2.7 (0.2)	43.4 (1.0)
708	$FeCl_2$	1.2 (0.7)	62.8 (13.3)	28.4 (15.7)	7.8 (2.6)
708	(Zn, Fe)S	50.3 (0.8)	n.d.	22.6 (3.2)	26.9 (3.2)
825	(Zn, Fe)S	50.7 (0.2)	n.d.	18.3 (1.4)	31.0 (1.2)
825	(Fe, Zn)S	50.2 (0.3)	n.d.	28.3 (0.5)	21.5 (0.3)
825	FeS	50.8 (0.5)	n.d.	48.7 (0.6)	0.4 (0.1)
1005	(Zn, Fe)S	50.4 (0.3)	n.d.	14.7 (0.9)	34.8 (0.6)
1005	(Fe, Zn)S	50.1 (0.2)	n.d.	22.1 (0.8)	27.8 (1.0)

Notes. Standard deviations of the analyses are given in brackets. Backscattered electron images of the analyzed phases are shown in Figures 3 and 4; n.d., not detected, that is, below the detection limit.

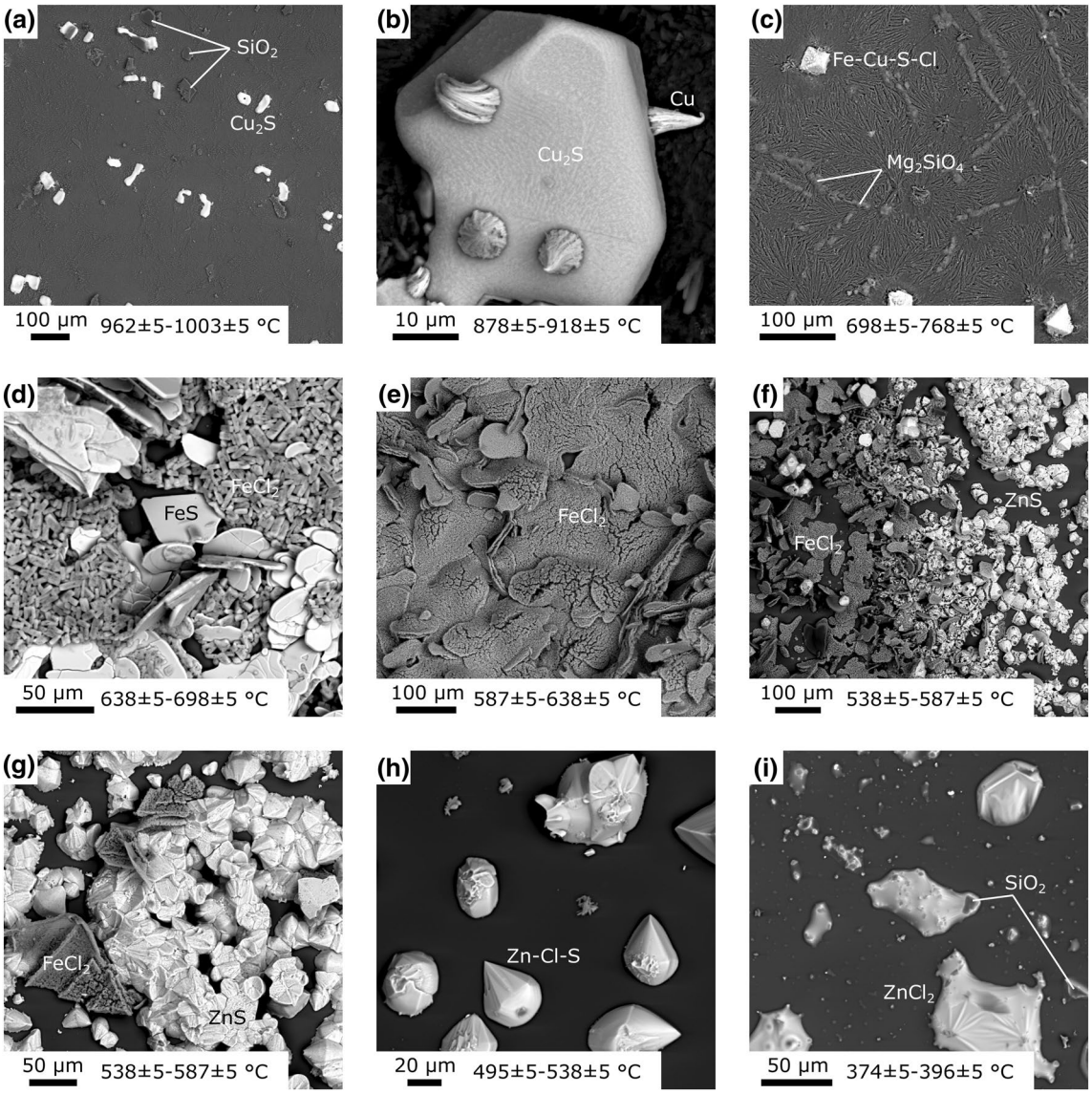

Figure 2. Backscattered electron images of phases deposited on the inner silica tube wall ("gas deposition experiment"). (a) Cu_2S grains and SiO_2 glass dust which was formed during opening of the tube, 962 ± 5–1,003 ± 5°C; (b) Cu_2S grain with Cu metal whiskers, 878 ± 5–918 ± 5°C; (c) Un-identified Fe-Cu-S-Cl phase and Mg_2SiO_4, the reaction product of MgO with the silica glass tube wall, 698 ± 5–768 ± 5°C; (d) FeS and $FeCl_2$, 638 ± 5–698 ± 5°C; (e) $FeCl_2$, 587 ± 5–638 ± 5°C; (f) $FeCl_2$ and ZnS, 538 ± 5–587 ± 5°C; (g) $FeCl_2$ and ZnS, 538 ± 5–587 ± 5°C; (h) Un-identified Zn-Cl-S phase, 495 ± 5–538 ± 5°C; (i) Liquidized and hydrated $ZnCl_2$ due to its deliquescence, SiO_2 glass shards, 374 ± 5–396 ± 5°C.

3.2. Metal Reaction Experiments

The Fe metal chips reacted with a C-O-S-Cl-Zn gas at 396 ± 10, 496 ± 10, 580 ± 10, 708 ± 10, 825 ± 10, and 1005 ± 10°C, and the run products show that the reaction resulted in extensive reaction coatings with variable amounts of $FeCl_2$, (Zn,Fe)S and FeS (Table 4). In Figures 4 and 5, we show backscattered electron images of the surface coatings on the metal chips and polished cross-sections of the coated Fe metal chips. With increasing temperature, the coatings become thicker and coarser grained (Figure 5). This proved to be problematic during the sample polishing of the cross-sections for SEM analysis, as the sulfide coatings partially decoupled from the underlying Fe metal chips.

At 396 ± 10°C, the coating almost exclusively contains $FeCl_2$ (lawrencite) which crystallized as prismatic crystals with lengths of up to 200 µm and thicknesses of up to 40 µm (Figure 4a). On the surface coatings, we did not observe any sulfide phase. In cross-section, it is evident that the coatings are thin with thick-

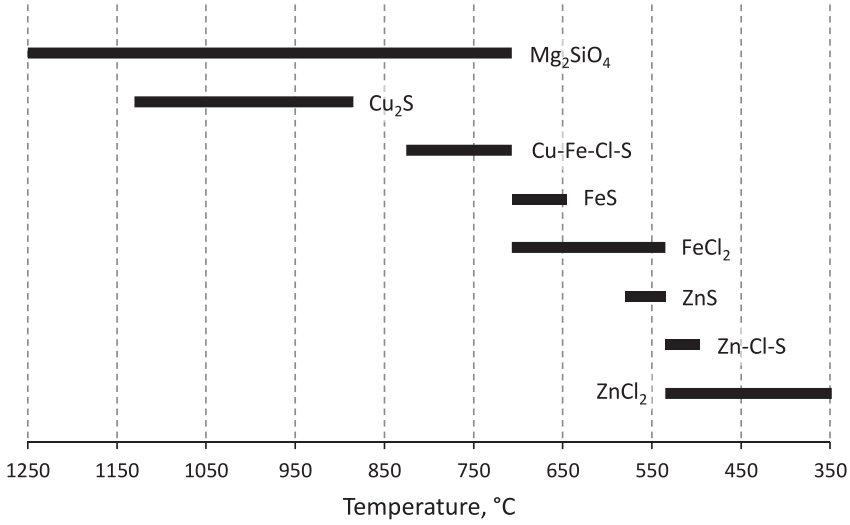

Figure 3. Distribution of phases deposited along the temperature gradient in the silica tube summarizing the observations shown in Figure 2 from the gas deposition experiment. The solid bars show the temperature ranges over which the respective phases were observed in the silica glass tube by investigation of the inner tube wall with back-scattered electron microscopy and EDS analysis. "Rusty Rock" phases are observed over the temperature range 538 ± 5–638 ± 5°C. EDS, Energy-Dispersive X-Ray spectroscopy.

nesses of up to 20 μm (Figures 4a and 4b). In addition to lawrencite, we also detected traces of S by EDS. However, we could not observe individual grains.

At 496 ± 10°C, lawrencite forms a dense and fine-grained coating on the reacted Fe metal (Figure 4d). Individual grains are small with diameters of less than 5 μm. In cross-section, we observe that the coating is much thicker than at 396 ± 10°C, measuring up to 80 μm (Figures 4e and 4f). We also observe reaction between the lawrencite and the epoxy resin in which the sample is embedded (Figure 4f). This secondary alteration of the coating likely occurred during embedding in the liquid resin as it did not change once the resin hardened.

At 580 ± 10°C, we observe $FeCl_2$ and (Zn,Fe)S in the coating of the Fe metal chip (Figure 4g). The coating is fine-grained with individual (Zn, Fe) S crystals with diameters of up to 8 μm. The coating has partially engulfed silica glass fibers on which the Fe metal chip was placed (Figure 4g). In cross-section, we observe that the coating with a thickness of up to 150 μm partially detached from the metal, suggesting a poor cohesion (Figures 4h and 4i). The coating appears to be layered, with the $FeCl_2$ on the metal chip and the sulfide on the surface (Figure 4i).

At 708 ± 10°C, (Zn, Fe)S dominates the coating and only traces of $FeCl_2$ are observed in cross-section (Figures 5a–5c). The sulfide grains have diameters of up to 40 μm (Figure 5a), with a total coating thickness of ~100 μm (Figure 5b). Traces of $FeCl_2$ were detected in the coating by EDS, but individual grains could not be identified unambiguously, suggesting grain sizes of less than 2 μm.

At 825 ± 10°C, the coating only contains sulfides. It is the only sample where pure FeS could be distinguished from (Zn, Fe) S. At the surface of the coating, grains have diameters of up to 60 μm (Figure 5d). The coating is dense and the individual sulfide crystals are euhedral. The coating is partially detached from the underlying Fe metal chip (Figure 5e), but, in some sections, the contact is observed. The pure FeS is in direct contact with the metal chip and forms an undulatory interface (Figure 5f). The (Zn, Fe) S occurs on the surface of the coating.

Finally, at 1005 ± 10°C, the coating mainly consists of (Fe, Zn)S (Figures 5g–5i). The sulfide grains have diameters of up to 50 μm. The coating thickness exceeds 200 μm and was mostly lost during preparation of the cross-sections (Figure 5h). The surface of the reacted Fe metal chip is highly undulatory and porosity is observed to a depth of 200 μm (Figures 5h and 5i). The pore space formed during the reaction with the

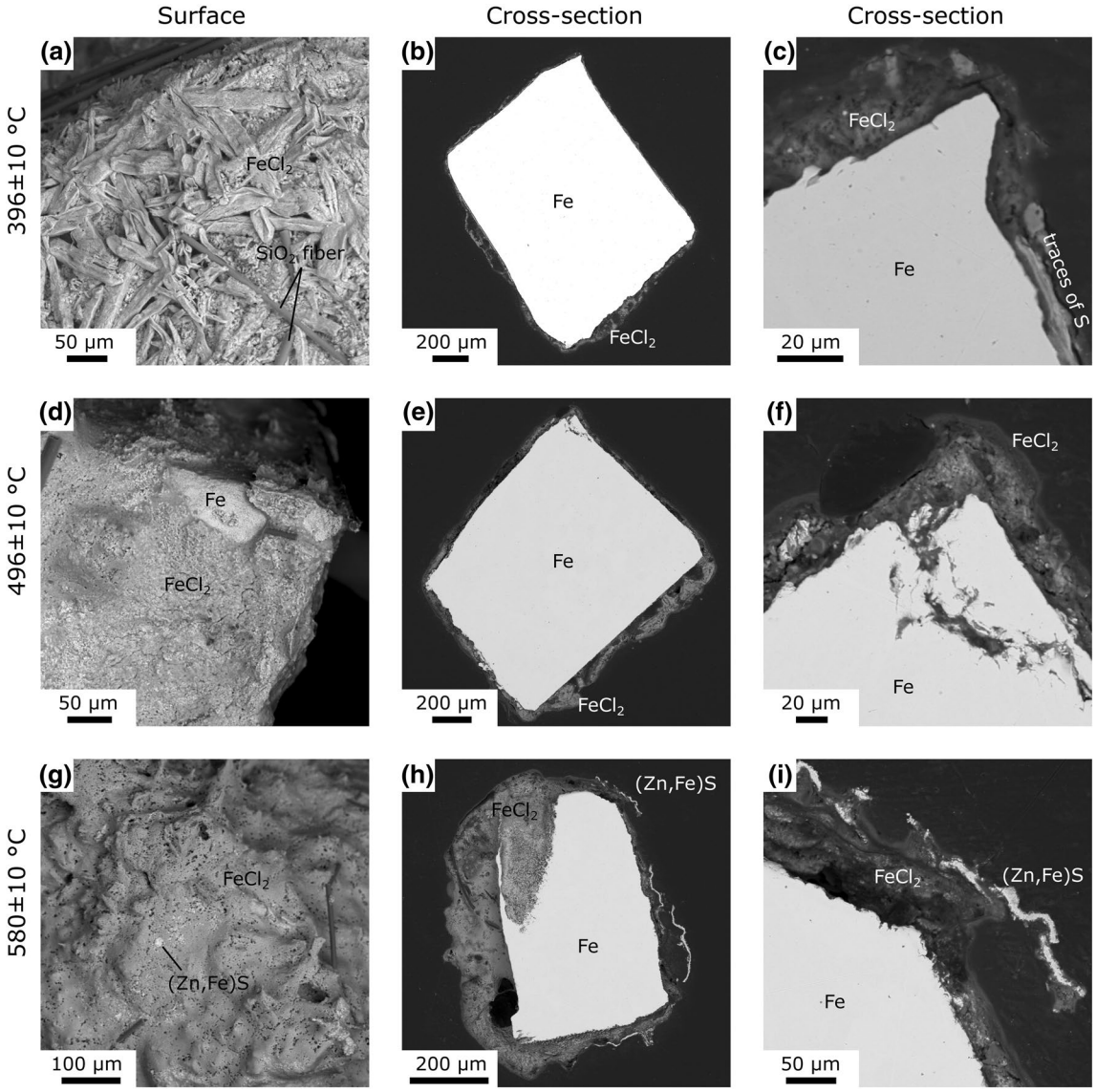

Figure 4. Backscattered electron images of the Fe metal reaction experiment. Images a, d, and c show the surfaces of the coatings and images b, c, e, f, h, and i show cross-sections of the samples. The rows indicate the temperatures, 396 ± 10°C (a)–(c), 496 ± 10°C (d)–(f), and 580 ± 10°C (g)–(h).

C-O-S-Cl-Zn gas suggests a mobilization of Fe at 1005 ± 5°C. Indeed, apart from (Fe, Zn) S we also observe fayalite (Fe_2SiO_4) in the coating (Figures 5g and 5i). The fayalite is primarily located where the Fe metal chip was in contact with the silica glass wool or the wall of the silica glass tube, facilitating the reaction.

In summary, 580 ± 10°C is the only temperature at which both $FeCl_2$ and (Zn, Fe)S could be observed abundantly in the coatings. At lower temperatures only traces of sulfide could be detected in the coatings, whereas at 708 ± 10°C only traces of $FeCl_2$ were detected. At even higher temperatures (825 ± 10, 1005 ± 10°C), chlorides are absent from the coatings.

4. Discussion

Both the "gas deposition experiments" and the "metal reaction experiments" result in the formation of mineral assemblages containing sulfides and chlorides, and both experimental approaches reproduce the fumarolic alteration products observed in the lunar Apollo 16 "Rusty Rock" 66095. In the gas deposition

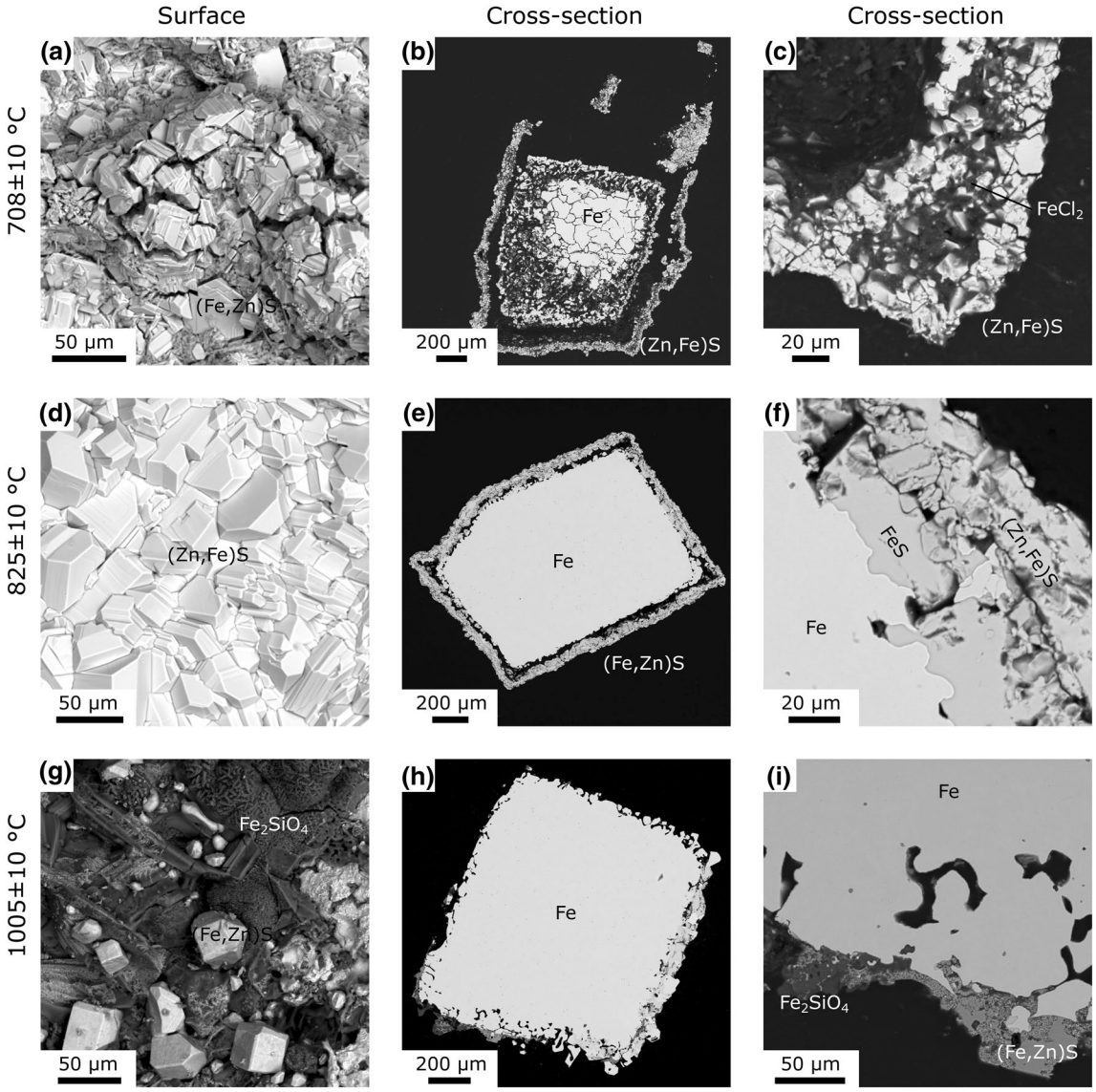

Figure 5. Backscattered electron images of the Fe metal reaction experiment. Images a, d, and c show the surfaces of the coatings and images b, c, e, f, h and i show cross-sections of the samples. The rows indicate the temperatures, 708 ± 10°C (a)–(c), 825 ± 10°C (d)–(f), and 1,005 ± 10°C (g)–(h).

experiments, FeS, $FeCl_2$, and ZnS occur over the temperature range of 538–638 ± 5°C. In the metal reaction experiment, the most extensive reaction and formation of both (Zn, Fe) S and $FeCl_2$ occurred at 580 ± 10°C, which is an almost identical temperature range as the gas deposition experiment. The two experiments suggest that 580 ± 50°C is the temperature condition under which fumarolic alteration occurred on the Moon, as recorded in the "Rusty Rock" samples.

In our dry high temperature experiments, we did not observe any oxyhydroxides and oxides that have been reported in the Apollo "Rusty Rock" samples, such as akaganéite (β-FeO [OH, Cl]), goethite (α-FeO [OH]), or hematite (α-Fe_2O_3; Shearer et al., 2014). We conducted our experiments with water free, dried reagents, following the proposed H-poor nature of the C-O-S-Cl gas phase (Norman et al., 1995; Shearer et al., 2012, 2014). Our experiments have consistently reproduced the dry alteration phases observed in the "Rusty Rock". This suggests that the oxyhydroxides are a secondary alteration product of the primary $FeCl_2$ formed at high temperature. The textural evidence from the Apollo 16 sample suggests that oxyhydration did not form upon exposure to a terrestrial atmosphere, but that akaganéite did replace lawrencite, based on the

Cl-isotopes (Shearer et al., 2014). This suggests that the initial fumarolic alteration phase at 580 ± 50°C was followed by a secondary alteration phase at lower temperatures and with a gas at higher fH_2 and fH_2O.

We performed our experiments in sealed and evacuated silica tubes with a 900°C temperature range. In such an experimental setup, the direct control of gas fugacities (e.g., fO_2 and fS_2) is not possible in the same way as in a conventional gas mixing furnace. Furthermore, the gas fugacities may vary along the temperature gradient, as well as over time as phases are deposited from the gas phase or gas species are bound to solids via chemisorption (King et al., 2018; Nekvasil et al., 2019). In addition, gas-solid reaction experiments may be kinetically limited (Renggli and King, 2018), as they are in nature (King et al., 2018). However, the large temperature gradient, variations in gas fugacities with temperature and time, as well as pressure increase with volatilization of elements at high temperature, followed by a pressure degrease as phases deposit from the gas at lower temperatures, are analogous to natural fumarolic processes (Henley & Seward, 2018). We argue that our experimental approach adequately represents these natural systems (Renggli and Klemme, 2020). Furthermore, some first-order estimates on the gas composition can be made based on the phases observed in the experiments and in the lunar "Rusty Rock".

4.1. Constraints on the Gas Phase Composition

As mentioned above, the starting material used in our experiments contained graphite powder (Table 1) and it was placed in graphite crucibles. Graphite acts as a strong reducing agent and limits the fO_2 at the source at 1240°C, as any free oxygen will react with the excess graphite to form CO gas. This is in analogy to the formation of CO-rich lunar volcanic gas that was argued to have formed by the oxidation of graphite (Fogel & Rutherford, 1995; Nicholis & Rutherford, 2009). The CO-bearing gas includes gaseous Zn and O due to the decomposition of ZnO and reaction with graphite. A second decomposition process follows the equations $ZnO + MgCl_2 = ZnCl_{2(g)} + MgO$ or $ZnO + MgCl_2 = Zn_{(g)} + Cl_{2(g)} + MgO$, but these do not directly impinge on the oxygen fugacity.

At lower temperatures, gas compositions, or gas fugacities, are assessed based on the phase assemblages observed in the experiments and the lunar "Rusty Rock." First, we discuss the "gas deposition experiments." All chalcocite crystals deposited between 880 and 1140°C show the growth of Cu metal whiskers on the surface (Figures 2a and 2b). Metal whiskers on sulfides are an indication of a decrease in fS_2 after the formation of the sulfides in a low pressure environment (Nicolle & Rist, 1979; Wagner, 1952). For example, iron whiskers were observed on sulfide grains in samples from asteroid 25,143 Itokawa, sampled by Hayabusa (Matsumoto et al., 2020). The observation of Cu metal whiskers on the Cu_2S grains illustrates that the gas fugacities in our runs are not constant over time. Initially, the Zn-Cu-Fe-C-O-S-Cl compounds in the source volatilize rapidly which results in increasing gas pressure in the silica glass tube. As sulfides and chlorides deposit from the gas phase along the temperature gradient the gas pressure decreases again. The sole species remaining abundantly in the gas phase is CO, controlled by the reaction of excess graphite with any available oxygen in the source at 1240°C. The formation of the Cu metal whiskers suggests that $\log fS_2$ drops to the phase boundary of Cu_2S and Cu in the $\log fS_2$-$\log fO_2$ space, as indicated by the arrow in Figure 6a. In addition, the absence of any oxidized Fe-phases suggests that $\log fO_2$ did not increase above the Fe-FeO buffer.

The occurrence of FeS and $FeCl_2$ together in both experimental approaches in the temperature range 580 ± 50°C, which we identified as the temperature condition forming the "Rusty Rock" alteration on the Moon, allows further constraints of $\log fS_2$ and $\log fCl_2$ in the experiment and for the lunar "Rusty Rock." The presence of both FeS and $FeCl_2$ (Figure 2d for the gas deposition experiment and Figure 4i for the metal reaction experiment) constrains the two variables to the univariate line indicated in Figure 6b. At 600°C, $\log fS_2$ is in the range of −13.2 to −10.5 and $\log fCl_2$ is in the range of −13.9 to −12.5 (Figure 6b).

Finally, in the Fe "metal reaction experiments," the redox state, at least in the colder parts of the tube, is further constrained by the Fe metal chips at 396 ± 10, 496 ± 10, 580 ± 10, 708 ± 10, 825 ± 10, and 1005 ± 10°C. As we did not observe any oxidized iron in the experiments, we conclude that the $\log fO_2$ remained below the IW buffer at all temperatures and for the entire duration of the experiment.

Recent calculations of a lunar volcanic gas phase revealed that main gas species are S_2, CO, and H_2 at 1200°C, 10^{-6} bar and reducing conditions of IW-2 (C. J. Renggli et al., 2017). This model was based on meas-

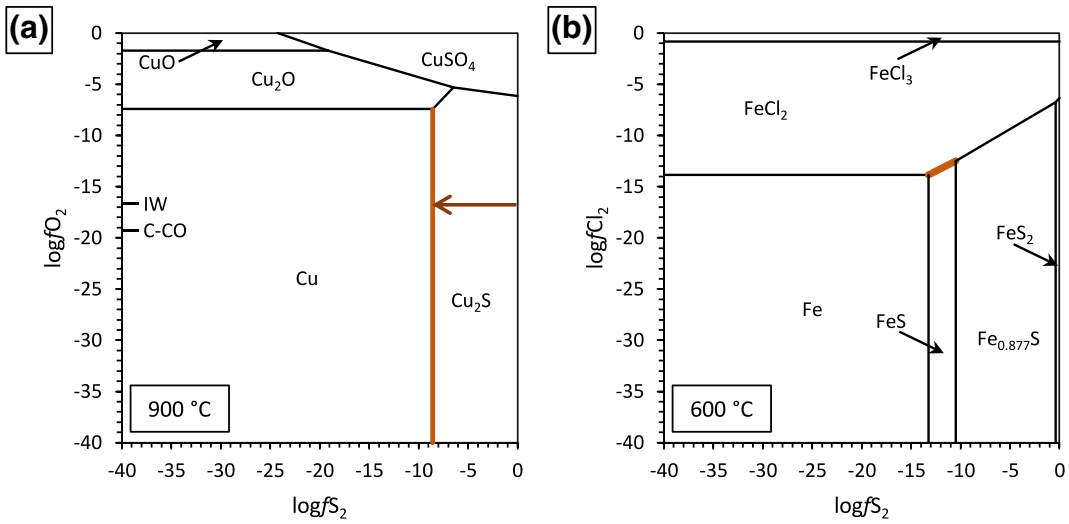

Figure 6. (a) Phase stability diagram of the system Cu-S-O as a function of $\log fS_2$ and $\log fO_2$ at 900°C, 1 bar. The univariate line in brown shows the condition for coexistence of Cu and Cu_2S as observed in the metal transport experiment and the formation of Cu whiskers on the Cu_2S crystal. The brown arrow indicates a decrease in $\log fS_2$ with experimental duration resulting in the growth of Cu whiskers. (b) Phase stability diagram of the system Fe-S-Cl as a function of $\log fS_2$ and $\log fCl_2$ at 600°C, 1 bar. The univariate line shows the co-stability of $FeCl_2$ and FeS as observed in the metal transport experiment at 638 ± 5–698 ± 5°C (Figure 2d) and the Fe metal-gas reaction experiment at 580 ± 10°C (Figures 4g–4i). Calculations were made with the program HSC9 by Outotec, largely based on data from the NIST-JANAF thermochemical data base (Chase, 1998; Roine, 2015).

urements of the volatiles H, S, Cl, F, and C in partially degassed lunar pyroclastic glass beads (Saal et al., 2008; Wetzel et al., 2015). In such a volcanic gas composition, the metals primarily deposit as sulfides with only minor abundances of elemental metal. Zinc, Fe, Ni, and Cu were observed as sulfides in coatings on the pyroclastic glass beads and the only chloride that was observed was NaCl (Butler & Meyer, 1976; Cirlin & Housley, 1979; Clanton et al., 1978; Wasson et al., 1976). Iron and Zn-chlorides, as observed in the Apollo 16 "Rusty Rock," and, in our experiments, are not predicted as deposited solids in the thermodynamic model and were not observed in pyroclastic glass bead coatings (C. J. Renggli et al., 2017). As a consequence, we suggest that the gas composition forming the "Rusty Rock" alteration had a different composition than the volcanic gas driving pyroclastic eruptions. Specifically, the $\log fCl_2$ must have been orders of magnitude higher in the "Rusty Rock" alteration environment, compared to the pyroclastic gas, allowing the deposition of metal chlorides from the gas phase and the reaction of Fe metal in the host rock to chloride. Commonly used 50% condensation temperatures (Lodders, 2003) suggest deposition of Fe above 1300°C (Day et al., 2019). However, our experimental results showed that $FeCl_2$ are deposited from a gas phase at temperatures as low as 540°C. This underlines the importance of experimental exploration of a broader range of gas compositions from which metals deposit and condensate in planetary environments. Finally, in our experiments, the relative abundances of Fe-, Zn-, and Cu-phases were limited by the addition of these metals to the starting materials in equal molar abundances (Table 1). These abundances do not represent those in the lunar samples, but were chosen to allow a better comparison of the behavior of these metals in our experiments.

Note that the sulfide mineralization was not just observed in the Apollo 16 "Rusty Rock" but sulfides have been observed in other Apollo 16 samples, including 67016 (Norman, 1981; Norman et al., 1995; Shearer et al., 2012), as well as Apollo 11, 14, and 17 rocks (Elardo et al., 2012; McKay et al., 1972; Ramdohr, 1972). However, these rocks do not show chloride alteration and the predominant sulfide phase is troilite (Shearer et al., 2012). In our experiment, FeS was deposited from the gas phase at 638 ± 5–698 ± 5°C (Figure 3). In addition to sulfide veins, likely deposited from a reducing S-rich gas, troilite also occurs in metasomatic replacement textures of olivine to troilite and low-Ca pyroxene (Colson, 1992; Norman et al., 1995; Shearer et al., 2012). In an ongoing study, we will further investigate the conditions under which these metasomatic replacement reactions occurred. At more oxidizing conditions, sulfates rapidly form when SO_2 reacts with

basaltic glasses and minerals (King et al., 2018; K. P. L. Renggli, Henley et al., 2019). At reducing conditions relevant to the Moon and Mercury (Blewett et al., 2013; Nittler et al., 2014), sulfides are predicted to form in a S-rich environment. At 700°C and an oxygen fugacity < IW additional sulfides may form including Na-, Ca-, and Mg-sulfides (P. A. B. Renggli, King, et al., 2019b).

5. Conclusions

We conducted gas deposition and metal reaction experiments to simulate fumarolic alteration in the Apollo 16 "Rusty Rock" 66095. The silica glass tube experiments are a useful tool to explore metal transport processes and gas-solid reactions, such as sulfidation processes. Our experiments indicate that the observed mineral assemblage of the "Rusty Rock" was formed at 580 ± 50°C. In this temperature range, we observed the deposition of $FeCl_2$, ZnS, and FeS in the gas deposition experiment, and the formation of $FeCl_2$ and (Zn, Fe) S coatings on Fe metal grains reacted with a Zn-C-O-S-Cl gas. The gas deposition experiments also showed that Cu_2S was deposited at higher temperatures above 880°C. Consequently, if Cu was carried in the lunar fumarolic gas, it must have been deposited at higher temperatures and therefore likely at greater depths in the lunar crust compared to the "Rusty Rock" alteration. This result supports the hypothesis that Cu was not introduced into the "Rusty Rock" by a fumarolic gas, but was already present in the host rock, as suggested by the normal lunar mare basalt δ^{65}Cu composition (Day et al., 2019). Our experiments do not allow us to discriminate between the deposition of $FeCl_2$ and FeS from the fumarolic gas versus the in situ reaction of metallic iron with a C-O-S-Cl gas. Both processes result in the formation of $FeCl_2$ and FeS in the temperature range of 580 ± 50°C. The observed assemblage of $FeCl_2$ and FeS, and the absence of oxidized iron, allowed us to constrain sulfur and chlorine fugacities in the gas phase at reducing conditions below the IW buffer. At 600°C, $\log fS_2$ is at −13.5 to −10.5 and $\log fCl_2$ is at −13.9 to −12.5.

Data Availability Statement

No additional data were used in the preparation of this manuscript.

Acknowledgments
Renggli is supported by a SNSF Early Postdoc. Mobility fellowship P2SKP2_181367. This research was partially supported by DFG project 263649064 – SFB TRR-170, publication number 125. Our thanks also go to M. Feldhaus, P. Weitkamp, L. Buxtrup, A. Hardes, and S. Flunkert for help and support in the laboratories at WWU Münster. The authors thank Bradley Thomson for the editorial handling of this manuscript, and Gokce Ustunisik, Malcolm Rutherford, and Hanna Nekvasil for their helpful reviews that significantly improved this manuscript. Open access funding enabled and organized by Projekt DEAL.

References

Blewett, D. T., Vaughan, W. M., Xiao, Z., Chabot, N. L., Denevi, B. W., Ernst, C. M., et al. (2013). Mercury's hollows: Constraints on formation and composition from analysis of geological setting and spectral reflectance. *Journal of Geophysical Research: Planets*, *118*(5), 1013–1032. https://doi.org/10.1029/2012je004174

Butler, P., & Meyer, C. (1976). Sulfur prevails in coatings on glass droplets - Apollo 15 green and brown glasses and Apollo 17 orange and black (devitrified) glasses. In *Lunar Science Conference*, Paper presented at Proceedings of the Seventeenth Lunar and Planetary Science Conference (Vol. 7, pp. 1561–1581). New York, NY: Pergamon Press. Retrieved from https://ui.adsabs.harvard.edu/abs/1976LPSC....7.1561B/abstract

Chase, M. W. (1998). *NIST-JANAF thermochemical tables*, Journal of physical and chemical reference data (4th ed.). Woodbury, N.Y.: American Chemical Society.

Cirlin, E. H., & Housley, R. M. (1979). Scanning Auger Microprobe and atomic absorption studies of lunar volcanic volatiles. In *Lunar and Planetary Science Conference* (Vol. 10, pp. 341–354). New York, N.Y.: Pergamon Press.

Clanton, U. S., McKay, D. S., Waits, G., & Fuhrman, R. (1978). Sublimate morphology on 74001 and 74002 orange and black glassy droplets. *Lunar and Planetary Science Conference*. Paper presented at Lunar and Planetary Science Conference (Vol. 9, pp. 1945–1957). New York, NY: Pergamon Press.

Colson, R. O. (1992). Mineralization on the Moon?: Theoretical considerations of Apollo 16 "rusty rocks," sulfide replacement in 67016, and surface-correlated volatiles on lunar volcanic glass. *Proceedings of Lunar and Planetary Science*. Paper presented at Proceedings of Lunar Planetary Science (Vol. 22, pp. 427–436). Houston, TX: Lunar and Planetary Institute.

Dalby, K. N., Berger, J. A., Brand, H. E. A., Cairney, J. M., Eder, K., Eggins, S. M., et al. (2018). Analytical techniques for probing small-scale layers that preserve information on gas–solid interactions. *Reviews in Mineralogy and Geochemistry*, *84*, 103–175.

Day, J. M. D., Moynier, F., & Shearer, C. K. (2017). Late-stage magmatic outgassing from a volatile-depleted Moon. *Proceedings of the National Academy of Sciences*, *114*(36), 9547–9551. https://doi.org/10.1073/pnas.1708236114

Day, J. M. D., Sossi, P. A., Shearer, C. K., & Moynier, F. (2019). Volatile distributions in and on the Moon revealed by Cu and Fe isotopes in the 'Rusty Rock' 66095. *Geochimica et Cosmochimica Acta*, *266*, 131–143. https://doi.org/10.1016/j.gca.2019.02.036

El Goresy, A., Ramdohr, P., Pavićević, M., Medenbach, O., Müller, O., & Gentner, W. (1973). Zinc, lead, chlorine and FeOOH-bearing assemblages in the Apollo 16 sample 66095: Origin by impact of a comet or a carbonaceous chondrite? *Earth and Planetary Science Letters*, *18*, 411–419.

Elardo, S. M., McCubbin, F. M., & Shearer, C. K. (2012). Chromite symplectites in Mg-suite troctolite 76535 as evidence for infiltration metasomatism of a lunar layered intrusion. *Geochimica et Cosmochimica Acta*, *87*, 154–177.

Fogel, R. A., & Rutherford, M. J. (1995). Magmatic volatiles in primitive lunar glasses: I. FTIR and EPMA analyses of Apollo 15 green and yellow glasses and revision of the volatile-assisted fire-fountain theory. *Geochimica et Cosmochimica Acta*, *59*, 201–215.

Gargano, A., Sharp, Z., Shearer, C., Simon, J. I., Halliday, A., & Buckley, W. (2020). The Cl isotope composition and halogen contents of Apollo-return samples. *Proceedings of the National Academy of Sciences*, *117*(38), 23418–23425. http://dx.doi.org/10.1073/pnas.2014503117

Haskin, L. A., & Warren, P. (1991). Lunar chemistry. In G. H. Heiken, D. T. Vaniman, & B. V. French (Eds.), *Lunar source book* (pp. 357–474). New York, NY: Cambridge University Press.

Henley, R. W., & Seward, T. M. (2018). Gas–solid reactions in arc volcanoes: Ancient and modern. *Reviews in Mineralogy and Geochemistry*, *84*, 309–349.

Hunter, R. H., & Taylor, L. A. (1981a). Rust and schreibersite in Apollo 16 highland rocks: Manifestations of volatile-element mobility. In *Lunar and Planetary Science Conference* (Vol. 12, pp. 253–259). New York and Oxford: Pergamon Press.

Hunter, R. H., & Taylor, L. A. (1981b). Rusty rock 66095: A paradigm for volatile-element mobility in highland rocks. In *Lunar and Planetary Science Conference*. Paper presented at Lunar and Planetary Science Conference Proceedings (Vol. 12, pp. 261–280). New York, NY, Oxford, UK: Pergamon Press.

Jean, M. M., Bonder, B., Farley, C., & Taylor, L. A. (2016). "Rusty rocks" from the moon: Volatile-element contributions from meteorites. In *Lunar and Planetary Science Conference* (Vol. 47, p. 2498). Houston, TX: Lunar and Planetary Institute. Retrieved From http://adsabs.harvard.edu/abs/2016LPI....47.2498J

Kerridge, J. F., Kaplan, I. R., Petrowski, C., & Chang, S. (1975). Light element geochemistry of the Apollo 16 site. *Geochimica et Cosmochimica Acta*, *39*, 137–162.

King, P. L., Wheeler, V. M., Renggli, C. J., Palm, A. B., Wilson, S. A., Harrison, A. L., et al. (2018). Gas–solid reactions: Theory, experiments and case studies relevant to earth and planetary processes. *Reviews in Mineralogy and Geochemistry*, *84*, 1–56.

Krähenbühl, U., Ganapathy, R., Morgan, J. A., & Anders, E. (1973). Volatile elements in Apollo 16 samples: Implications for highland volcanism and accretion history of the moon. In *Proceedings of the Lunar Science Conference* (Vol. 4, pp. 1325–1348). New York, NY: Pergamon Press.

Lodders, K. (2003). Solar system abundances and condensation temperatures of the elements. *The Astrophysical Journal*, *591*, 1220.

Matsumoto, T., Harries, D., Langenhorst, F., Miyake, A., & Noguchi, T. (2020). Iron whiskers on asteroid Itokawa indicate sulfide destruction by space weathering. *Nature Communications*, *11*, 1–8.

McCubbin, F. M., Kaaden, K. E. V., Tartèse, R., Klima, R. L., Liu, Y., Mortimer, J., et al. (2015). Magmatic volatiles (H, C, N, F, S, Cl) in the lunar mantle, crust, and regolith: Abundances, distributions, processes, and reservoirs. *American Mineralogist*, *100*, 1668–1707.

McKay, D. S., Clanton, U. S., Morrison, D. A., & Ladle, G. H. (1972). Vapor phase crystallization in Apollo 14 breccia. In *Proceedings of the Lunar Science Conference* (Vol. 3, pp. 739–752). New York: Pergamon Press.

Meyer, C. (2009). 66095 "rusty rock". In *Lunar Sample Compendium*. Houston, TX: Astromaterials Research & Exploration Science (ARES). Retrieved from https://curator.jsc.nasa.gov/lunar/lsc/

Nekvasil, H., DiFrancesco, N. J., Rogers, A. D., Coraor, A. E., & King, P. L. (2019). Vapor-deposited minerals contributed to the martian surface during magmatic degassing. *Journal of the Geophysical Research: Planets*, *124*, 1592–1617. https://doi.org/10.1029/2018je0059

Nicholis, M. G., & Rutherford, M. J. (2009). Graphite oxidation in the Apollo 17 orange glass magma: Implications for the generation of a lunar volcanic gas phase. *Geochimica et Cosmochimica Acta*, *73*, 5905–5917.

Nicolle, R., & Rist, A. (1979). The mechanism of whisker growth in the reduction of wüstite. *Metallurgical Transactions B*, *10*, 429–438.

Nittler, L. R., Weider, S. Z., Starr, R. D., Chabot, N., Denevi, B. W., Ernst, C. M., et al. (2014). Sulfur-depleted composition of Mercury's largest pyroclastic deposit: Implications for explosive volcanism and surface reflectance on the innermost planet. In *Lunar and Planetary Science Conferenc* (Vol. 45, pp. 1391). Houston, TX: Lunar Planetary Institute.

Norman, M. D. (1981). Petrology of suevitic lunar breccia 67016. In *Lunar Planetary Science Conference* (Vol. 12, pp. 235–252). New York, NY, Oxford, UK: Pergamon Press.

Norman, M. D., Keil, K., Griffin, W. L., & Ryan, C. G. (1995). Fragments of ancient lunar crust: Petrology and geochemistry of ferroan noritic anorthosites from the Descartes region of the Moon. *Geochimica et Cosmochimica Acta*, *59*, 831–847.

Norris, C. A., & Wood, B. J. (2017). Earth's volatile contents established by melting and vapourization. *Nature*, *549*, 507–510.

Papike, J. J., Taylor, L. A., & Simon, S. (1991). Lunar minerals. In G. H. Heiken, D. T. Vaniman, & B. V. French (Eds.), *Lunar source book* (pp. 357–474). New York, NY: Cambridge University Press.

Ramdohr, P. (1972). Lunar pentlandite and sulfidization reactions in microbreccia 14315, 9. *Earth and Planetary Science Letters*, *15*, 113–115.

Renggli, K. P. L., Henley, R. W., Guagliardo, P., McMorrow, L., Middleton, J. P., & Turner, M. (2019a). An experimental study of SO_2 reactions with silicate glasses and supercooled melts in the system anorthite–diopside–albite at high temperature. *Contributions to Mineralogy and Petrology*, *174*, 3.

Renggli, C. J., & King, P. L. (2018). SO_2 gas reactions with silicate glasses. *Reviews in Mineralogy and Geochemistry*, *84*, 229–255.

Renggli, P. A. B., King, P. L., & Guagliardo, P. (2019b). Implications of reactions between SO_2 and basaltic glasses for the mineralogy of planetary crusts. *Journal of the Geophysical Research: Planets*, *124*(10), 2563–2582. https://doi.org/10.1029/2019je006045

Renggli, C. J., King, P. L., Henley, R. W., & Norman, M. D. (2017). Volcanic gas composition, metal dispersion and deposition during explosive volcanic eruptions on the Moon. *Geochimica et Cosmochimica Acta*, *206*, 296–311.

Renggli, C. J., & Klemme, S. (2020). Experimental constraints on metal transport in fumarolic gases. *Journal of Volcanology and Geothermal Research*, *400*, 106929.

Roine, A. (2015). *Outotec HSC chemistry 8.1*, Pori, Finland: Outotec Research Center.

Saal, A. E., Hauri, E. H., Cascio, M. L., Van Orman, J. A., Rutherford, M. C., & Cooper, R. F. (2008). Volatile content of lunar volcanic glasses and the presence of water in the Moon's interior. *Nature*, *454*, 192–195.

Sharp, Z. D., Shearer, C. K., McKeegan, K. D., Barnes, J. D., & Wang, Y. Q. (2010). The chlorine isotope composition of the moon and implications for an anhydrous mantle. *Science*, *329*, 1050–1053.

Shearer, C. K., Burger, P. V., Guan, Y., Papike, J. J., Sutton, S. R., & Atudorei, N.-V. (2012). Origin of sulfide replacement textures in lunar breccias. Implications for vapour element transport in the lunar crust. *Geochimica et Cosmochimica Acta*, *83*, 138–158.

Shearer, C. K., Sharp, Z. D., Burger, P. V., McCubbin, F. M., Provencio, P. P., Brearley, A. J., & Steele, A. (2014). Chlorine distribution and its isotopic composition in "rusty rock" 66095. Implications for volatile element enrichments of "rusty rock" and lunar soils, origin of "rusty" alteration, and volatile element behaviour on the Moon. *Geochimica et Cosmochimica Acta*, *139*, 411–433.

Sossi, P. A., & Fegley, B. (2018). Thermodynamics of element volatility and its application to planetary processes. *Reviews in Mineralogy and Geochemistry*, *84*, 393–459.

Sossi, P. A., Klemme, S., O'Neill, H. S C., Berndt, J., & Moynier, F. (2019). Evaporation of moderately volatile elements from silicate melts: Experiments and theory. *Geochimica et Cosmochimica Acta*, *260*, 204–231.

Taylor, L. A., Mao, H. K., & Bell, P. M. (1973). "Rust" in the Apollo 16 rocks. In *Proceedings of the Lunar Science Conference* (Vol. 4, pp. 829–839). Houston, TX: Lunar and Planetary Institute.

Taylor, L. A., Mao, H. K., & Bell, P. M. (1974). Identification of the hydrated iron oxide mineral Akaganéite in Apollo 16 lunar rocks. *Geology*, *2*, 429–432.

Ustunisik, G., Nekvasil, H., Lindsley, D. H., & McCubbin, F. M. (2015). Degassing pathways of Cl-, F-, H-, and S-bearing magmas near the lunar surface: Implications for the composition and Cl isotopic values of lunar apatite. *American Mineralogist*, *100*, 1717–1727.

Wagner, C. (1952). Mechanism of the reduction of oxides and sulphides to metals. *The Journal of The Minerals, Metals & Materials Society*, *4*, 214–216.

Wang, Y., Guan, Y., Hsu, W., & Eiler, J. M. (2012). Water content, chlorine and hydrogen isotope compositions of lunar apatite. *Meteoritics & Planetary Science Supplement*, *75*, 5170.

Wasson, J. T., Boynton, W. V., Kallemeyn, G. W., Sundberg, L. L., & Wai, C. M. (1976). Volatile compounds released during lunar lava fountaining. In *Lunar and Planetary Science Conference* (Vol. 7, pp. 1583–1595). Houston, TX: Lunar Planetary Institute.

Wetzel, D. T., Hauri, E. H., Saal, A. E., & Rutherford, M. J. (2015). Carbon content and degassing history of the lunar volcanic glasses. *Nature Geoscience*, *8*, 755–758.

Zelenski, M., Kamenetsky, V. S., Taran, Y., & Kovalskii, A. M. (2020). Mineralogy and origin of aerosol from an arc basaltic eruption: Case study of Tolbachik volcano, Kamchatka. *Geochemistry, Geophysics, Geosystems*, *21*, e2019GC008802. https://doi.org/10.1029/2019gc008802